THE JOURNAL OF PHYSICAL CHEMISTRY A
A JOURNAL OF THE AMERICAN CHEMICAL SOCIETY

pubs.acs.org/JPCA

Article

Modeling Photolytic Decomposition of Energetically Functionalized Dodecanes

Tammie Nelson,* Patricia L. Huestis, and Virginia W. Manner*

Cite This: J. Phys. Chem. A 2022, 126, 7094−7101

Read Online

ACCESS | Metrics & More | Article Recommendations | Supporting Information

ABSTRACT: The photolytic stability of explosives and energetic functional groups is of importance for those who regularly handle or are exposed to explosives in typical environmental conditions. This study models the photolytic degradation of dodecane substituted with various energetic functional groups: azide, nitro, nitrate ester, and nitramine. For the studied molecules, it was found that excitons localize on the energetic functional group, no matter where they were initially formed, and thus, the predominant degradation pathway involves the degradation of the energetic functional group. The relative trends for both 4 and 8 eV excitation energies followed with what is expected from the relative stability of the energetic functional groups to thermal and sub-shock degradation. The one notable exception was the azide functional group; more work should be done to further understand the photolytic effects on the azide functional group.

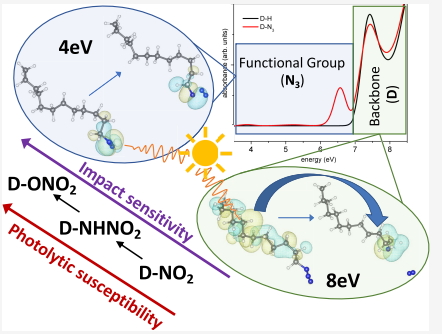

INTRODUCTION

Photolytic degradation of explosives is of interest for a variety of settings, from environmental remediation of contaminated sites[1] to the handling of explosives in sunlight. While many experiments have been conducted on the photolysis of various explosive contaminants in water, the mechanisms of degradation can be especially elusive. For this reason, computational studies on the photolytic degradation of explosives are important. Here, we present the first example of a study where a consistent molecular backbone has been utilized in order to systematically evaluate photolysis effects on different energetic functional groups.

Thousands of explosives exist, with numerous combinations of energetic functional groups, making it impossible to investigate the photolytic response of each. Instead, this study investigates a few commonly used energetic functional groups; namely, azide (N_3), nitro (NO_2), nitrate ester (ONO_2), and nitramine ($NHNO_2$). These energetic functional groups are attached to dodecane ($C_{12}H_{26}$) such that each molecule has a common backbone allowing the relative photolytic stability to be directly compared among the different energetic functional groups by eliminating the effects of the backbone structure. Though these materials are not explosives, this approach will allow us to probe what could happen in organic explosives subjected to photolysis conditions; in particular, it will allow for understanding both degradation pathways in the ultraviolet (UV) energy regime and will allow us to rank the susceptibility of these energetic functional groups to photolytic degradation. Additionally, the photolytic decomposition of dodecane and other liquid alkane chains have been explored extensively,[2−7] thus allowing benchmarking of the computational approach against experimental results.

Here, we introduce the **D−X** notation used to refer to the dodecane systems studied in this work. **D** = $\mathbf{C_{12}H_{25}}$ and **X** = **H** or the energetic functional group. In this notation, dodecane would be **D−H**. The chemical structures for the studied molecules can be seen in Figure 1.

COMPUTATIONAL METHODS

Nonadiabatic Molecular Dynamics. In order to model the photolytic degradation, the dynamics following photoexcitation (exciton generation via photon absorption) is followed using nonadiabatic molecular dynamics (NAMD)[8] implemented within the nonadiabatic excited state molecular dynamics (NEXMD) software.[9] There are many NAMD methods and codes available, each with their own strengths and weaknesses depending on the system and physical processes of interest (see recent reviews[8,10]). NEXMD is unique in its ability to treat large systems (10−100s of atoms) with multiple excited states (100 states) on relatively long time scales (ps). NEXMD uses the fewest switches surface hopping (FSSH) algorithm[11] to efficiently model the nonradiative relaxation through multiple coupled electronic excited states in large molecular systems. An ensemble of independent

Received: May 16, 2022
Revised: September 20, 2022
Published: October 5, 2022

https://doi.org/10.1021/acs.jpca.2c03404
J. Phys. Chem. A 2022, 126, 7094−7101

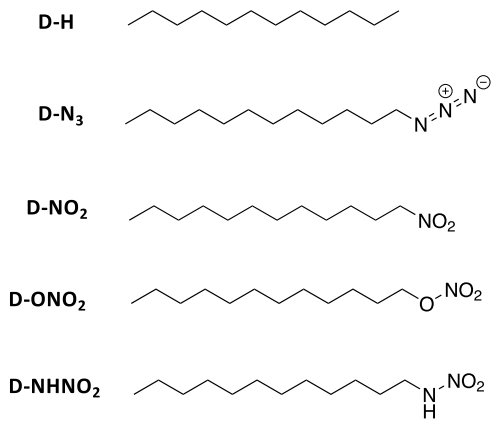

Figure 1. Chemical structure of studied molecules: unfunctionalized dodecane (**D−H**); dodecane with terminal functionalization of azide (**D−N$_3$**), nitro (**D−NO$_2$**), nitrate ester (**D−ONO$_2$**), and nitramine (**D−NHNO$_2$**). **D** = $C_{12}H_{25}$.

trajectories is propagated and, within each trajectory, the nuclei are treated classically with forces from a single adiabatic excited state potential energy surface (PES). Transitions (hops) among coupled states depend on the strength of the nonadiabatic couplings. Meanwhile, electrons are described quantum mechanically requiring the calculation of excited state energies, analytical gradients, and nonadiabatic couplings.[12−17] The collective electronic oscillator (CEO) approach[18,19] is used to compute excited states at the configuration interaction singles (CIS)[20] level of theory coupled with the semiempirical AM1 Hamiltonian[21] to decrease the numerical demand associated with treating large molecular systems. We benchmark our AM1/CIS level of theory by comparing calculated UV−vis absorption spectra to experimental spectra measured by us (Figure S1) and comparing the calculated density of excited states for AM1/CIS to TD-DFT using the hybrid PBE0 functional (Figure S2). It is relevant to note that although the dynamical rates produced by NAMD simulations are very sensitive to the calculated energy gaps,[22] the mechanistic information depends on the electronic character of states (i.e., spatial localization) and do not depend strongly on energy gaps. Because we are interested in the decomposition pathways rather than timescales, the qualitative agreement between calculated and experimental UV−vis absorption spectra (Figure S1) and TD-DFT and CIS density of excited states (Figure S2) is sufficient for our purpose. The spin unrestricted open-shell CIS implementation of NEXMD provides more accurate reaction barriers.[23] Due to the absence of the spin−orbit coupling in the present NEXMD implementation, the dynamics for both open- and closed-shell simulations is followed only in the singlet manifold with no intersystem crossing.

Simulation Details. We start by running a ground-state (GS) MD trajectory of each molecule in Figure 1 starting from the GS minimum energy structure. GS dynamics were performed using constant temperature Langevin propagation[24,25] at 300 K with a time step of 0.5 fs and friction coefficient of 20 ps^{-1}. From each of the equilibrated GS trajectories, N_{config} snapshots of nuclear geometries and velocities were sampled at 1 ps intervals to provide initial conditions for subsequent excited state dynamics. For each sampled configuration, excited state energies and oscillator strengths were computed for 200 lowest energy excited states (including both singlet and triplet spin states) to produce an average absorption spectrum. The contribution to the total spectrum from each excited state is modeled using a Gaussian lineshape with spectral broadening of 0.1 eV. The length of the GS trajectory and N_{config} values are provided in Table S1 (Supporting Information) for each molecule.

For each molecule, NAMD simulations were performed for low and high energy excitation. N_{config} corresponds to the number of NAMD trajectories, where each trajectory starts from a different configuration and appropriately chosen excited state. The initial excited state for each NAMD trajectory was selected stochastically according to a Gaussian-shaped Frank-Condon window centered at either 4 or 8 eV for low or high energy simulations, respectively. A Gaussian laser pulse was used, $f(t) = \exp(-t^2/2\ T^2)$, with T = 42.5 fs corresponding to a FWHM of 100 fs. Excited state trajectories were then propagated for up to 1 ps with a classical time step of 0.1 fs and a quantum time step of 0.025 fs. The nonadiabatic dynamics are performed at constant energy such that all excess electronic energy is converted into nuclear kinetic energy by adjusting the velocity of all nuclei in the direction of the nonadiabatic coupling vector. Nuclear degrees of freedom are not quantized (i.e., excess electronic energy is evenly distributed to all nuclei) and there is no dissipation of kinetic energy. The number of excited states included in each simulation N_S^{NAMD} is given in Table S1 for each molecule. The instantaneous decoherence correction[26] was used to account for divergent wave packets, and trivial unavoided crossings were detected by reducing the quantum time step by a factor of 40.[27,28] The 4 eV simulations utilized an open-shell electronic structure model for excited state dynamics, while the 8 eV simulations used a closed-shell electronic structure model. While the open-shell model is more accurate, it is too computationally expensive to perform the 8 eV dynamics with an open-shell representation. The closed-shell simulations at 8 eV already require the calculation of hundreds of singlet excited states.

Analysis of Degradation Pathways and Transition Densities. In order to analyze the decomposition pathways occurring in the molecules following an electronic excitation, bond distances were tracked in every NAMD trajectory. Bond breaking thresholds, provided in Table S2, are set following our previous work.[29] If the separation between any two atom pairs exceeds the set threshold and remains above the threshold until the end of the trajectory, the bond is considered broken. The quantum yield (QY) for a given decomposition pathway is calculated as the fraction of NAMD trajectories in which the given bond breaking event occurs. Note that the calculated QY will not necessarily sum to 1 because not all trajectories result in bond breaking within the simulated timescale; the energy can be dissipated to vibrational heating without resulting in bond breaking.

During NAMD simulations, the exciton localization and spatial energy transfer can be followed via the time-dependent localization of the electronic transition density. The orbital representation of the diagonal elements, $(\rho_{0\alpha})_{nn} = \langle\varphi_0|c_n^\dagger c_n|\varphi_\alpha\rangle$,[30,31] in atomic orbital (AO) basis functions n, provides a convenient analysis of the excited state wave function distribution in space. Here, ϕ_0 and ϕ_α are the ground and excited state adiabatic wave functions, respectively, and $c_n^\dagger c_n$ are the creation/annihilation operators on the AOs. By partitioning the dodecane **D−X** molecules into **D** and **X** units corresponding to the dodecane chain and the energetic

https://doi.org/10.1021/acs.jpca.2c03404
J. Phys. Chem. A 2022, 126, 7094−7101

functional group, the fraction of transition density, $[\rho^{0\alpha}(t)]^2_U$, localized on each unit (U) at any given time is calculated by summing the contributions of the AOs from each atom (A) in a unit according to $[\rho^{0\alpha}(t)]_U{}^2 = \sum_{n_A m_A} [\rho^{0\alpha}{}_{n_A m_A}(T)]^2$.

RESULTS

Absorption Spectra. First, we analyze the calculated UV−vis absorption spectrum for the studied molecules, as shown in Figure 2. According to our calculated spectra (Figure 2), the

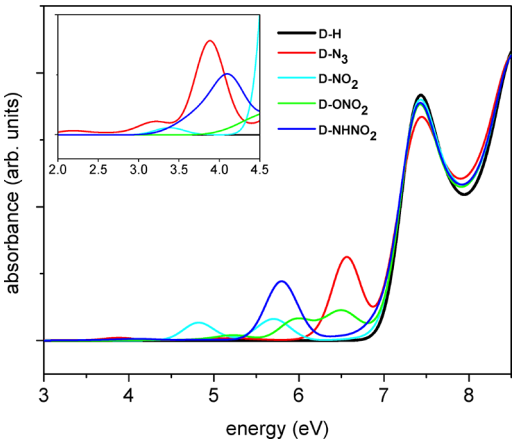

Figure 2. Calculated absorption spectra for studied molecules; inset shows rescaled low energy (<4 eV) portion of spectrum.

onset of absorption in unfunctionalized dodecane **D**−**H** (bold black line) occurs near 7 eV, indicating that the peaks in the spectral region above 7 eV in functionalized dodecanes correspond to the alkane chain. Peaks below 7 eV appear only in functionalized dodecanes, indicating that the low energy region of the spectrum corresponds to the functional group. The comparison of the density of excited states for functionalized and unfunctionalized dodecanes (Figure S2) provides a consistent interpretation. Because of this difference in excited state character (i.e., localization), 4 and 8 eV were chosen for photolytic calculations. The low energy excitation at 4 eV targets the energetic functional group while the high energy excitation at 8 eV targets the alkane backbone. The excitation energies in relation to the density of excited states can be seen in Figure S2.

Initial Exciton Localization and Energy Transfer. Next, we consider the exciton localization and energy transfer between dodecane **D** and the energetic functional group **X** units by analyzing the average fraction of transition density (TD) localized in each unit during the photoexcited dynamics. The time-evolution of the fraction of TD in each unit shown in Figure 3 for **D**−$\mathbf{N_3}$ is averaged separately over the subset of trajectories that undergo a N−N_2 bond break and the subset of trajectories that do not break. The corresponding molecular orbital plots for initial and final snapshots from a representative trajectory are also shown. The electronic transition density gives a good representation of the exciton localization. From these plots, it is clear that the exciton is initially generated on the energetic functional group at low energy (4 eV) excitation. Because the lowest energy electronic states are associated with the energetic group (see Figure 2), the exciton remains localized in the energetic group and no spatial energy transfer occurs. The situation is different for high energy (8 eV) excitation. Here, the exciton is initially localized in the

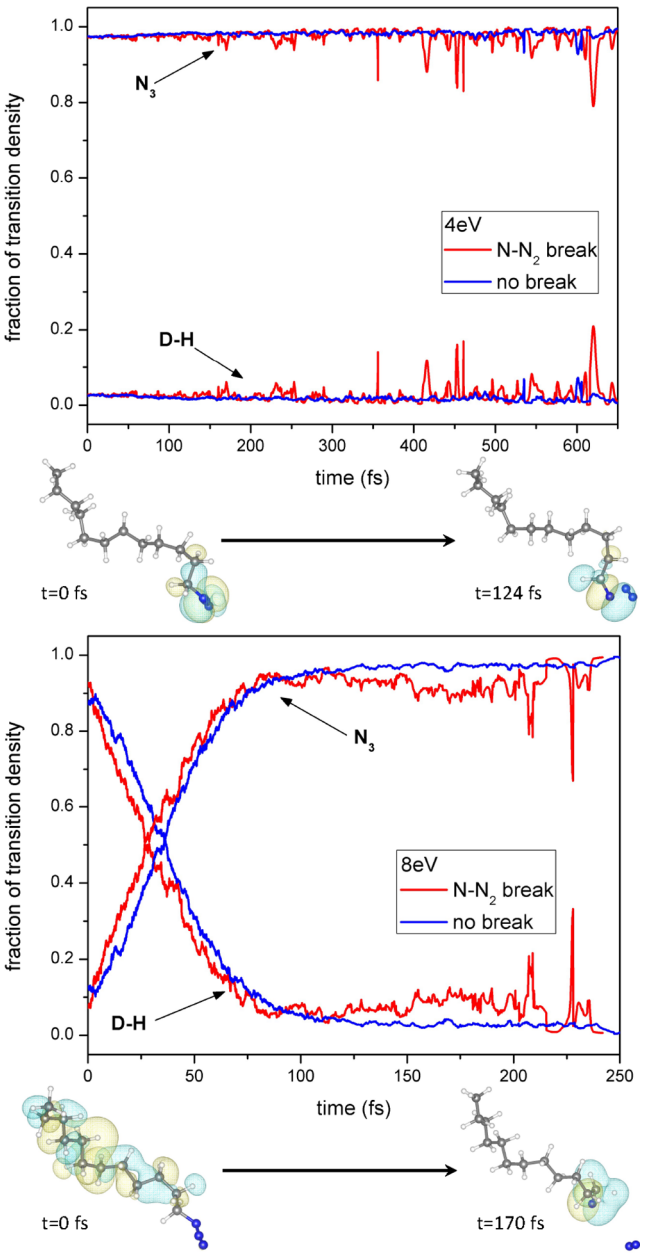

Figure 3. Exciton localization for **D**−$\mathbf{N_3}$ revealed by the time evolution of the fraction of TD localized in dodecane **D** and energetic functional group $\mathbf{N_3}$ units during NAMD simulations at 4 eV (**top**) and 8 eV (**bottom**) averaged over the subset of trajectories that undergo breakage of the N−N_2 bond (red line) and the subset of trajectories that do not undergo degradation (blue line). Molecular orbital plots from a representative trajectory show initial and final exciton localizations.

dodecane **D** unit and quickly undergoes a spatial energy transfer to the energetic functional group concomitant with the relaxation to lower energy electronic states.

While **D**−$\mathbf{N_3}$ was chosen as a representative example to illustrate the energy transfer and change in exciton localization, the other molecules displayed the same behavior at high and low excitation energies, and their plots can be found in the Supporting Information (Figure S3). For all functionalized molecules, the 4 eV excitation remained localized on the energetic functional group where it was initially created, while the 8 eV excitation was initially localized on the dodecane

https://doi.org/10.1021/acs.jpca.2c03404
J. Phys. Chem. A 2022, 126, 7094−7101

Table 1. Degradation Pathways and Quantum Yields (QY) at 4 and 8 eV Excitation Energies[a]

molecule	4 eV pathway (QY)	8 eV pathway (QY)
D−H	NA	D−H → D° + H_2 (0.45) D−H → D + $H^{+/-}$ (0.022) D−H → D˝ + CH_4 (0.002) D−H → D† + CH_3CH_2 (0.002)
$D-N_3$	D−N_3 → D−N + N_2 (0.235) D−N_3 → D + N_3 (0.002)	D−N_3 → D−N + N_2 (0.396) D−N_3 → D + N_3 (0.01) D−N_3 → D°−N_3 + $H^{+/-}$ (0.018) D−N_3 → D* + CH_2N_3 (0.007)
$D-NO_2$	D−NO_2 → D + NO_2 (0.301) D−NO_2 → D−NO + O (0.001)	D−NO_2 → D + NO_2 (0.187)
$D-ONO_2$	D−ONO_2 → D−O + NO_2 (0.651)	D−ONO_2 → D−O + NO_2 (0.405) D−ONO_2 → D°−O + NO_2 + $H^{+/-}$ (0.003)
$D-NHNO_2$	D−$NHNO_2$ → D−NH + NO_2 (0.577) D−$NHNO_2$ → D−N + NO_2 + H+/·/− (0.001)	D−$NHNO_2$ → D−NH + NO_2 (0.288) D−$NHNO_2$ → D−NNO_2 + $H^{+/-}$ (0.007)

[a]D = $C_{12}H_{25}$; D° = $C_{12}H_{24}$; D˝ = $C_{11}H_{22}$; D† = $C_{10}H_{21}$; D* = $C_{11}H_{23}$.

backbone and underwent an ultrafast spatial energy transfer to the energetic functional group. This phenomenon was true for all subsets of trajectories regardless of whether or not degradation occurred.

Decomposition Pathways. Table 1 summarizes the decomposition pathways for each compound and lists the corresponding QY. It is important to note that the sum of the QYs will not necessarily be one; the molecule can also undergo internal conversion via pathways that do not involve decomposition. The initial and final snapshots from NAMD simulations are shown in Figure 4 for the most probable pathways and Figures S4−S8 (Supporting Information) show initial and final snapshots for all pathways listed in Table 1.

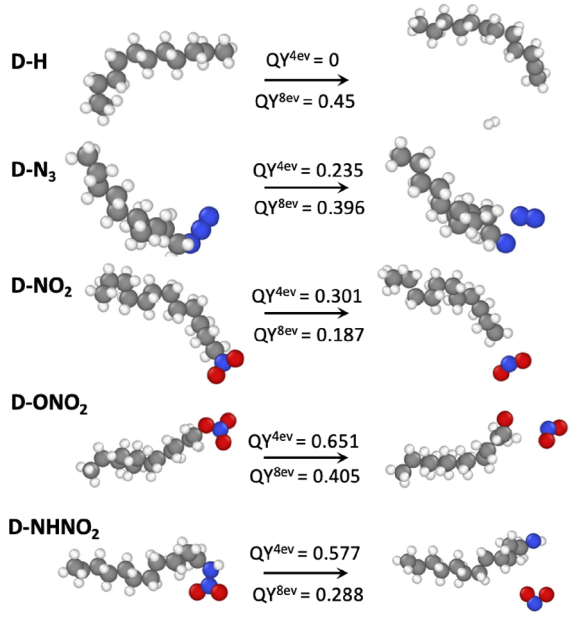

Figure 4. Initial and final snapshots from NAMD simulations for the most probable decomposition pathways in the molecules of interest. Representative snapshots are taken from 8 eV trajectories but observed pathways and products are the same for both 4 and 8 eV simulations. QY at 4 and 8 eV excitation energies are shown above and below arrow, respectively. Note that the reaction in (**D−H**) occurs only at 8 eV. Also note that comparisons of the QY across energies are not valid.

It is important to note that comparisons of the QYs between 4 and 8 eV simulations are not possible due to the use of open-shell and closed-shell electronic structure methods, respectively, which may change the relative barrier heights. Within each energy explored, however, the trends should remain valid. Additionally, for the open-shell (4 eV) simulations, a leaving H can be either a proton (H^+ = proton), a neutral H radical ($H^·$ = proton + electron), or a negatively charged H atom (H^- = proton + 2 electrons) because electrons in molecular orbitals are not forced to be paired together. The resolution of our simulations does not distinguish between $H^+/H^·/H^-$, and it may be possible that a combination of all pathways is possible. In closed-shell (8 eV) simulations, electrons are forced to be paired together so that either H^+ or H^- is cleaved from the molecule. In these calculations, neutral $H^·$ cannot form, even though that is certainly possible in an experimental setting. Going forward, the H products will be referred to as either $H^{+/·/-}$ (4 eV) or $H^{+/-}$ (8 eV).

Decomposition of Unfunctionalized Dodecane. For unfunctionalized dodecane (**D−H**), only high energy (8 eV) excitation dynamics were performed because the molecule is optically inactive below 7 eV (Figure 2). The most common decomposition pathway observed in our simulations for unfunctionalized dodecane following 8 eV excitation was the loss of hydrogen gas as H_2 (Figure 4) which had a QY of 0.45. $H^{+/-}$ elimination was seen with a QY of 0.022, and some C−C bond breaking of the alkyl chain also occurred with a combined QY of 0.004 (Figure S4). These results are consistent with vacuum UV photolysis experiments of liquid *n*-alkanes.[5,6]

We further investigate the mechanism of hydrogen dissociation in detail. The top panel of Figure 5 shows a histogram of H loss at different sites along the alkane chain for different types of dissociation events. As seen in Figure 5, hydrogen dissociation occurs at all C sites on the chain, but is more common in the center of the chain than at terminal positions. Experimentally, the QY of H_2 increases with the increase in chain length,[7] which could be explained by the current results. There are three mechanisms for H loss. The most common mechanism consists of two C−H bonds breaking from the same C atom to form H_2 gas (blue bars). This occurs with a QY of 0.447. Alternatively, H_2 gas can form when two C−H bonds from neighboring C atoms break (green bars). This is an extremely rare event with a QY of 0.003.

https://doi.org/10.1021/acs.jpca.2c03404
J. Phys. Chem. A 2022, 126, 7094−7101

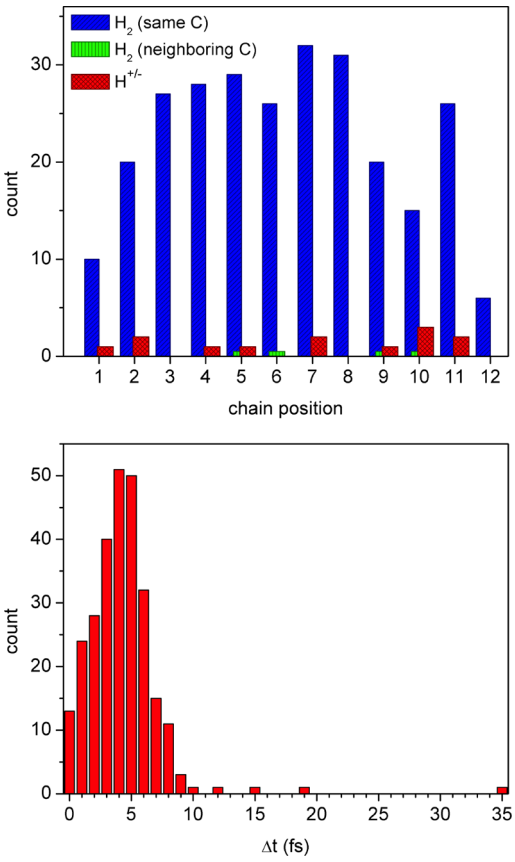

Figure 5. (**top**) Histogram of $H^{+/-}$ loss from unfunctionalized dodecane (**D−H**) at different C chain positions for three dissociation mechanisms. (**bottom**) Histogram of the time between proton dissociations, Δt, in unfunctionalized dodecane (**D−H**) for trajectories in which H_2 loss occurs (from the same or neighboring carbon atoms).

Finally, dissociation of a $H^{+/-}$ (red bars) occurs with a QY of 0.022. The vibrational period for the C−H stretching mode associated with the C−H bond breaking (assuming an equilibrium wavenumber of 3000 cm^{-1}) is 111.5 fs. The bottom panel of Figure 5 shows a histogram of the time between C−H cleavage events for trajectories in which H_2 loss occurs from either the same C or neighboring C. Because the C−H bonds always break within a fraction of a vibrational period, this can be considered as a single H_2 loss event rather than as two separate $H^{+/-}$ dissociations. The latter mechanism could produce reactive radical alkane intermediates; however, there is no evidence of this mechanism occurring in the present simulations.

Decomposition of Functionalized Dodecanes. We next analyze the decomposition pathways and QYs of the four functionalized compounds. For **D−N$_3$**, the most probable decomposition pathway at 4 eV is N_2 dissociation occurring with a QY of 0.235 (Figure 4), while dissociation of N_3 is a rare event occurring with a QY of 0.002 (Figure S5). At 8 eV excitation energy, the QYs of N_2 and N_3 dissociation are 0.396 and 0.01, respectively. In addition, new pathways involving the alkane chain are introduced with relatively low yields (Figure S5). $H^{+/-}$ loss from the carbon bonded to the energetic N_3 group occurs with a QY of 0.018 and dissociation of CH_2N_3 occurs with a QY of 0.007 leaving a shortened C_{11} alkane chain fragment.

For **D−NO$_2$**, **D−ONO$_2$**, and **D−NHNO$_2$**, the most probable decomposition pathway at both 4 and 8 eV is dissociation of NO_2 (Figure 4). At 4 eV, NO_2 dissociation occurs with a QY of 0.301 (**D−NO$_2$**), 0.651 (**D−ONO$_2$**), and 0.577 (**D−NHNO$_2$**). At 8 eV, these yields are 0.187 (**D−NO$_2$**), 0.405 (**D−ONO$_2$**), and 0.288 (**D−NHNO$_2$**). Relatively rare decomposition pathways are also observed in these compounds. At 4 eV, O dissociation from the NO_2 group was observed in **D−NO$_2$** with a QY of 0.001 (Figure S6). At 8 eV, $H^{+/-}$ dissociation from the carbon bonded to the energetic ONO_2 group was observed in **D−ONO$_2$** in conjunction with NO_2 dissociation with a QY of 0.003 (Figure S7). H dissociation from the amine in **D−NHNO$_2$** occurs either in conjunction with NO_2 dissociation (4 eV, H) or in isolation (8 eV, H) with a QY of 0.007 and 0.001, respectively (Figure S8). Note that for **D−NO$_2$** at 8 eV and **D−ONO$_2$** at 4 eV, only one pathway is shown in Table 1 because no other statistically significant pathways were observed within the limits of the sampled configurational space.

DISCUSSION

The exciton localization plots (Figure 3) confirm the choice of excitation energy selected from the analysis of Figure 2. 4 eV was chosen to target the energetic functional group, and that is where the exciton is localized for the entire computational duration. This fact is true for both trajectories that end in a bond break as well as those that do not end in a bond break. For the 8 eV trajectories, the exciton is initially localized on the alkane chain, as was expected. However, the exciton then transfers from the alkane chain to the energetic functional group. Again, this observation is true for both trajectories that end in a bond break as well as trajectories that do not end in a bond break. These results are not surprising because alkanes have demonstrated very efficient energy transfer processes along the C−C bonds of the main chain.[32,33] Although some of the 8 eV trajectories for the functionalized dodecane molecules (Table 1) suggest that the alkane chain can be degraded, these pathways are significantly less likely than degradation of the energetic functional group. In general, the exciton eventually localizes in the energetic functional group regardless of where it was initially formed, and the excess electronic energy from the exciton decay can dissipate to vibrational modes that degrade the energetic functional group. Here, and elsewhere, we have seen that the exciton must be spatially localized in the functional group in order for an energetic bond to break.[34] Therefore, the relative energy ordering between the functional group and backbone is a critical factor in photolytic degradation. In the molecules studied here, the lowest energy states are associated with the energetic functional group (see Figure 2). This means that at low excitation energies, the exciton is created directly on the functional group, allowing for bond breaking and energy transfer is not needed. At high excitation energies, energy transfer concomitant with electronic relaxation moves the exciton from high energy states localized on the dodecane backbone to low energy states localized on the energetic group, allowing bond breaking at the energetic sites. If the functional group was higher in energy than the backbone, then a low energy excitation would result in the degradation of only the backbone, and at high excitation energies, energy transfer would move the exciton to the backbone and the QY of the energetic group would likely decrease.

https://doi.org/10.1021/acs.jpca.2c03404
J. Phys. Chem. A 2022, 126, 7094−7101

For all of the functionalized dodecane QY results, the most probable decomposition pathway is the cleavage of the trigger linkage, or the weakest bond in an explosive molecule that is often thought to be responsible for explosive decomposition in the commonly used drop-weight impact test.[35−41] As a reminder, QY results between 4 and 8 eV are not comparable, but the results within each energy regime are. For materials containing azides, the trigger linkage is considered to be N−N_2.[37,42] For the nitro class explosives, the trigger linkage is thought to be the X−NO_2 bond where X = N, C, or O. Focusing just on the cleavage of the trigger linkages reveals an interesting pattern. For the 4 eV results, the QYs suggest the following trend from most susceptible to photolytic degradation to least susceptible: **D−ONO_2 → D−$NHNO_2$ → D−NO_2 → D−N_3**. For the 8 eV results, the trend is as follows: **D−ONO_2 → D−N_3 → D−$NHNO_2$ → D−NO_2**. It is interesting to note that the general trend for **D−ONO_2, D−$NHNO_2$,** and **D−NO_2** follows what is expected from the general trend of explosive sub-shock impact sensitivity for the various energetic functional groups. In general, it can be assumed that azides and nitrate esters will be the most sensitive, while nitros will be the least sensitive.[43−46] Although there is no current data to suggest that the photolytic stability should follow the same trend as explosive sensitivity, it is nonetheless an interesting result.

The one functional group that exhibits atypical behavior compared with explosive impact sensitivity in this analysis, especially at 4 eV, is the azide. It is known that the sensitivity of the azide functional group varies from completely insensitive (LiN_3) to highly sensitive ($Cu(N_3)_2$), and it is suggested that this effect could be due to the bonding structure within the functional group itself.[47] In this study, the **D−N_3** molecule has no difference in the bond distances between the two molecules at 4 and 8 eV. Properties within a single azide can also be counterintuitive. For instance, lead azide ($Pb(N_3)_2$) has a high thermal stability, but is also highly sensitive to impact and friction insults and will even explosively decompose before it melts.[48] This observation could potentially be explained by the abnormally high pre-exponential factor computed from Arrhenius plots of MD kinetic calculations,[49] even though this explanation seems insufficient for our calculations. In the MD kinetic calculations, the maximum energy probed was 0.2 eV, while our lowest energy was 4 eV. Obviously, the energy regime and how that energy was distributed throughout the molecule are very different in the two cases, and while a similar phenomenon could be present for photolysis, there is not yet enough data for conclusive statements. More work, including experimental verification, should therefore be completed to fully understand the peculiar azide photolysis results.

CONCLUSIONS

Overall, we have shown that degradation pathways and ranking for nitrate esters, nitramines, and nitro groups are comparable between photolysis results and thermal and sub-shock degradation. This is the first known systematic study that compares the photolytic stability of energetic functional groups using a consistent backbone structure. For the 4 and 8 eV results, we saw that although more degradation pathways became available at 8 eV, the predominant degradation pathway remained the same for the two energies. This result is likely due to the fact that energy deposited in the molecule, no matter where it is initially localized, travels to the energetic functional group. Lastly, the azide functional group photolysis degradation does not fall within the same ranking pattern as the other functional groups with respect to sub-shock sensitivity properties, which shows the importance of carefully evaluating and interpreting reactivity in different energy regimes.

ASSOCIATED CONTENT

Supporting Information

The Supporting Information is available free of charge at https://pubs.acs.org/doi/10.1021/acs.jpca.2c03404.

Simulation details for GS dynamics and NAMD trajectories; bond breaking thresholds for different atom pairs; comparison of experimental and calculated (AM1/CIS) UV−vis absorption spectra; comparison of calculated DOS using semiempirical (AM1) and hybrid TD-DFT (PBE0); time-evolution of the electronic transition density localization for D−NO_2, D−ONO_2, and D−$NHNO_2$; snapshots from NEXMD simulations for decomposition pathways in unfunctionalized dodecane (D−H) at 8 eV excitation energy; and snapshots from NEXMD simulations for decomposition pathways in functionalized dodecanes (D−N_3, D−NO_2, D−ONO_2, and D−$NHNO_2$) at 4 and 8 eV excitation energies (PDF)

AUTHOR INFORMATION

Corresponding Authors

Tammie Nelson − *Physics and Chemistry of Materials, Theoretical Division, Los Alamos National Laboratory, Los Alamos, New Mexico 87545, United States;* orcid.org/0000-0002-3173-5291; Email: tammien@lanl.gov

Virginia W. Manner − *High Explosives Science & Technology, Los Alamos National Laboratory, Los Alamos, New Mexico 87545, United States;* orcid.org/0000-0002-1916-4887; Email: vwmanner@lanl.gov

Author

Patricia L. Huestis − *High Explosives Science & Technology, Los Alamos National Laboratory, Los Alamos, New Mexico 87545, United States*

Complete contact information is available at: https://pubs.acs.org/10.1021/acs.jpca.2c03404

Notes

The authors declare no competing financial interest.

ACKNOWLEDGMENTS

The authors thank Marc Cawkwell for helpful discussions and acknowledge support from Campaign 8 Aging and Lifetimes Program. The work at Los Alamos National Laboratory (LANL) was performed using resources provided by the LANL Institutional Computing (IC) Program. LANL is operated by Triad National Security, LLC, for the National Nuclear Security Administration of the U.S. Department of Energy (Contract no. 89233218NCA000001). LA-UR-22-24079.

REFERENCES

(1) Pichtel, J. Distribution and Fate of Military Explosives and Propellants in Soil: A Review. *Appl. Environ. Soil Sci.* **2012**, *2012*, 617236.

(2) Okabe, H.; McNesby, J. R. Vacuum Ultraviolet Photolysis of Ethane: Molecular Detachment of Hydrogen. *J. Chem. Phys.* **1961**, *34*, 668−669.
(3) Okabe, H.; McNesby, J. R. Vacuum Ultraviolet Photochemistry. IV. Photolysis of Propane. *J. Chem. Phys.* **1962**, *37*, 1340−1346.
(4) McNesby, J. R.; Okabe, H. Vacuum Ultraviolet Photochemistry. *Adv. Photochem.* **1964**, *3*, 157−240.
(5) Schwarz, F. P.; Smith, D.; Lias, S. G.; Ausloos, P. The fluorescence and photofragmentation of liquid saturated hydrocarbons at energies above the photoionization threshold. *J. Chem. Phys.* **1981**, *75*, 3800−3808.
(6) Tagawa, S.; Hayashi, N.; Yoshida, Y.; Washio, M.; Tabata, Y. Pulse radiolysis studies on liquid alkanes and related polymers. *Int. J. Radiat. Appl. Instrum., Part C* **1989**, *34*, 503−511.
(7) Wojnarovitz, L. *Charged Particle and Photon Interactions with Matter*; 1st ed.; Mozumder, A., Hatano, Y., Eds.; CRC Press: Boca Raton, 2003; Chapter 13, pp 371−408.
(8) Nelson, T.; White, A. J.; Bjorgaard, J. A.; Sifain, A. E.; Zhang, Y.; Nebgen, B.; Fernandez-Alberti, S.; Mozyrsky, D.; Roitberg, A. E.; Tretiak, S. Non-adiabatic Excited-State Molecular Dynamics: Theory and Applications for Modeling Photophysics in Extended Molecular Materials. *Chem. Rev.* **2020**, *120*, 2215−2287.
(9) Malone, W.; Nebgen, B.; White, A.; Zhang, Y.; Song, H.; Bjorgaard, J. A.; Sifain, A. E.; Rodriguez-Hernandez, B.; Freixas, V. M.; Fernandez-Alberti, S.; et al. NEXMD Software Package for Nonadiabatic Excited State Molecular Dynamics Simulations. *J. Chem. Theory Comput.* **2020**, *16*, 5771−5783.
(10) Crespo-Otero, R.; Barbatti, M. Recent Advances and Perspectives on Nonadiabatic Mixed Quantum-Classical Dynamics. *Chem. Rev.* **2018**, *118*, 7026.
(11) Tully, J. Molecular Dynamics with Electronic Transitions. *J. Chem. Phys.* **1990**, *93*, 1061−1071.
(12) Tretiak, S.; Isborn, C.; Niklasson, A.; Challacombe, M. Representation Independent Algorithms for Molecular Response Calculations in Time-Dependent Self-Consistent Field Theories. *J. Chem. Phys.* **2009**, *130*, 054111.
(13) Tretiak, S.; Chernyak, V.; Mukamel, S. Recursive Density-Matrix-Spectral-Moment Algorithm for Molecular Nonlinear Polarizabilities. *J. Chem. Phys.* **1996**, *105*, 8914−8928.
(14) Furche, F.; Ahlrichs, R. Adiabatic Time-Dependent Density Functional Methods for Excited State Properties. *J. Chem. Phys.* **2002**, *117*, 7433−7447.
(15) Nelson, T.; Fernandez-Alberti, S.; Chernyak, V.; Roitberg, A. E.; Tretiak, S. Nonadiabatic Excited-State Molecular Dynamics Modeling of Photoinduced Dynamics in Conjugated Molecules. *J. Phys. Chem. B* **2011**, *115*, 5402−5414.
(16) Send, R.; Furche, F. First-Order Nonadiabatic Couplings from Time-Dependent Hybrid Density Functional Response Theory: Consistent Formalism, Implementation, and Performance. *J. Chem. Phys.* **2010**, *132*, 044107.
(17) Tavernelli, I.; Curchod, B. F. E.; Laktionov, A.; Rothlisberger, U. Nonadiabatic Coupling Vectors for Excited States within Time-Dependent Density Functional Theory in the Tamm-Dancoff Approximation and Beyond. *J. Chem. Phys.* **2010**, *133*, 194104.
(18) Mukamel, S.; Tretiak, S.; Wagersreiter, T.; Chernyak, V. Electronic Coherence and Collective Optical Excitations of Conjugated Molecules. *Science* **1997**, *277*, 781−787.
(19) Tretiak, S.; Mukamel, S. Density Matrix Analysis and Simulation of Electronic Excitations in Conjugated and Aggregated Molecules. *Chem. Rev.* **2002**, *102*, 3171−3212.
(20) Thouless, D. J. *The Quantum Mechanics Of Many-Body Systems*; Academic Press: New York, 1972.
(21) Dewar, M. J. S.; Zoebisch, E. G.; Healy, E. F.; Stewart, J. J. P. The development and use of quantum mechanical molecular models. 76. AMI: a new general purpose quantum mechanical molecular model. *J. Am. Chem. Soc.* **1985**, *107*, 3902.
(22) Freixas, V. M.; Nelson, T.; Ondarse-Alvarez, D.; Nijjar, P.; Mikhailovsky, A.; Zhou, C.; Fernandez-Alberti, S.; Bazan, G.; Tretiak, S. Experimental and theoretical study of energy transfer in a chromophore triad: What makes modeling dynamics successful? *J. Chem. Phys.* **2020**, *153*, 244114.
(23) Zhang, Y.; Li, L.; Tretiak, S.; Nelson, T. Nonadiabatic Excited-State Molecular Dynamics for Open-Shell Systems. *J. Chem. Theory Comput.* **2020**, *16*, 2053−2064.
(24) Paterlini, M.; Ferguson, D. Constant Temperature Simulations using the Langevin Equation with Velocity Verlet Integration. *Chem. Phys.* **1998**, *236*, 243−252.
(25) Attard, P. Statistical Mechanical Theory for Non-Equilibrium Systems. IX. Stochastic Molecular Dynamics. *J. Chem. Phys.* **2009**, *130*, 194113.
(26) Nelson, T.; Fernandez-Alberti, S.; Roitberg, A. E.; Tretiak, S. Nonadiabatic Excited-State Molecular Dynamics: Treatment of Electronic Decoherence. *J. Chem. Phys.* **2013**, *138*, 224111.
(27) Fernandez-Alberti, S.; Roitberg, A.; Nelson, T.; Tretiak, S. Identification of Unavoided Crossings in Nonadiabatic Photoexcited Dynamics Involving Multiple Electronic States in Polyatomic Conjugated Molecules. *J. Chem. Phys.* **2012**, *137*, 014512.
(28) Nelson, T.; Fernandez-Alberti, S.; Roitberg, A. E.; Tretiak, S. Artifacts due to trivial unavoided crossings in the modeling of photoinduced energy transfer dynamics in extended conjugated molecules. *Chem. Phys. Lett.* **2013**, *590*, 208−213.
(29) Nelson, T.; Bjorgaard, J.; Greenfield, M.; Bolme, C.; Brown, K.; McGrane, S.; Scharff, R. J.; Tretiak, S. Ultrafast Photodissociation Dynamics of Nitromethane. *J. Phys. Chem. A* **2016**, *120*, 519−526.
(30) Tretiak, S.; Chernyak, V.; Mukamel, S. Two-Dimensional Real-Space Analysis of Optical Excitations in Acceptor-Substituted Carotenoids. *J. Am. Chem. Soc.* **1997**, *119*, 11408−11419.
(31) Tretiak, S.; Chernyak, V.; Mukamel, S. Collective Electronic Oscillators for Nonlinear Optical Response of Conjugated Molecules. *Chem. Phys. Lett.* **1996**, *259*, 55−61.
(32) Partridge, R. H. Excitation energy transfer in alkanes. I. Exciton model. *J. Chem. Phys.* **1970**, *52*, 2485−2490.
(33) Partridge, R. H. Excitation energy transfer in alkanes. II. Experimental demonstration. *J. Chem. Phys.* **1970**, *52*, 2491−2500.
(34) Greenfield, M. T.; McGrane, S. D.; Bolme, C. A.; Bjorgaard, J. A.; Nelson, T. R.; Tretiak, S.; Scharff, R. J. Photoactive high explosives: linear and nonlinear photochemistry of petrin tetrazine chloride. *J. Phys. Chem. A* **2015**, *119*, 4846−4855.
(35) Wu, C. J. C.; Fried, L. E. First-principles study of high explosive decomposition energetics. *Eleventh International Detonation Symposium*; 1998, Vol. *4*.
(36) Song, X. S.; Cheng, X. L.; Yang, X. D.; He, B. Relationship between the bond dissociation energies and impact sensitivities of some nitro-explosives. *Propellants, Explos., Pyrotech.* **2006**, *31*, 306−310.
(37) Politzer, P.; Murray, J. S.; Lane, P. Computational determination of effects of electric fields upon "trigger linkages" of prototypical energetic molecules. *Int. J. Quantum Chem.* **2009**, *109*, 534−539.
(38) Harper, L. K.; Shoaf, A. L.; Bayse, C. A. Predicting Trigger Bonds in Explosive Materials through Wiberg Bond Index Analysis. *ChemPhysChem* **2015**, *16*, 3886−3892.
(39) Manner, V. W.; Cawkwell, M. J.; Kober, E. M.; Myers, T. W.; Brown, G. W.; Tian, H.; Snyder, C. J.; Perriot, R.; Preston, D. N. Examining the chemical and structural properties that influence the sensitivity of energetic nitrate esters. *Chem. Sci.* **2018**, *9*, 3649−3663.
(40) Duan, B.; Liu, N.; Lu, X.; Mo, H.; Zhang, Q.; Liu, Y.; Wang, B. Screening for energetic compounds based on 1,3-dinitrohexahydropyrimidine skeleton and 5-various explospheres: molecular design and computational study. *Sci. Rep.* **2020**, *10*, 18292.
(41) Joy, J.; Danovich, D.; Shaik, S. Nature of the Trigger Linkage in Explosive Materials Is a Charge-Shift Bond. *J. Org. Chem.* **2021**, *86*, 15588−15596.
(42) Shoaf, A. L.; Bayse, C. A. The effect of nitro groups on N2 extrusion from aromatic azide-based energetic materials. *New J. Chem.* **2019**, *43*, 15326−15334.
(43) Zeman, S.; Jungová, M. Sensitivity and Performance of Energetic Materials. *Propellants, Explos., Pyrotech.* **2016**, *41*, 426−451.

https://doi.org/10.1021/acs.jpca.2c03404
J. Phys. Chem. A 2022, 126, 7094−7101

(44) Cawkwell, M. J.; Manner, V. W. Ranking the Drop-Weight Impact Sensitivity of Common Explosives Using Arrhenius Chemical Rates Computed from Quantum Molecular Dynamics Simulations. *J. Phys. Chem. A* **2020**, *124*, 74−81.
(45) Lease, N.; Kay, L. M.; Brown, G. W.; Chavez, D. E.; Robbins, D.; Byrd, E. F. C.; Imler, G. H.; Parrish, D. A.; Manner, V. W. Synthesis of Erythritol Tetranitrate Derivatives: Functional Group Tuning of Explosive Sensitivity. *J. Org. Chem.* **2020**, *85*, 4619−4626.
(46) Cawkwell, M.; Ferreira, S.; Lease, N.; Manner, V. *Molecular Modeling of the Sensitivities of Energetic Materials*; 1st ed.; Elsevier BV., 2022; Vol. *22*; pp 347−367.
(47) Cartwright, M.; Wilkinson, J. Correlation of structure and sensitivity in inorganic azides i effect of non-bonded nitrogen nitrogen distances. *Propellants, Explos., Pyrotech.* **2010**, *35*, 326−332.
(48) Egghart, H. C. Properties of Lead Azide Prepared in Molten Salt Media. *Inorg. Chem.* **1967**, *6*, 2121−2122.
(49) Cawkwell, M. J.; Davis, J. V.; Lease, N.; Marrs, F. W.; Burch, A. C.; Ferreira, S. R.; Manner, V. W. Understanding explosive sensitivity with effective trigger linkage kinetics. *ACS Phys. Chem. Au.* **2022**, *2*, 448-458.

https://doi.org/10.1021/acs.jpca.2c03404
J. Phys. Chem. A 2022, 126, 7094−7101